PHYSICAL REVIEW B VOLUME 58, NUMBER 8 15 AUGUST 1998-II

Atomic resolution STM imaging of a twisted single-wall carbon nanotube

W. Clauss,* D. J. Bergeron, and A. T. Johnson
Department of Physics and Astronomy, University of Pennsylvania, 209 South 33rd Street, Philadelphia, Pennsylvania 19104
(Received 11 February 1998)

We present atomically resolved scanning tunneling microscopy images of single-wall carbon nanotubes (SWNT's) embedded in a crystalline nanotube rope. Although they may be interpreted as of a chiral nanotube, the images are more consistently explained as an achiral armchair tube with a quenched twist distortion. The existence of quenched twists in SWNT's in ropes might explain the fact that both as-grown bulk nanotube material and individual ropes have insulatorlike conductivity at low temperature. [S0163-1829(98)50532-2]

Nanostructured materials are an intriguing laboratory for investigating the properties of electrons and phonons in systems intermediate between solids and single atoms. The novel properties of sp^2-bonded elemental carbon make single-wall carbon nanotubes[1,2] (SWNT's) a particularly promising nanostructure with a remarkable number of proposed electronic, chemical, sensing, and mechanical applications. Since macroscopic amounts of atomically flawless SWNT's form spontaneously in a plasma containing appropriate catalyst atoms,[3] it is likely that some of these uses will soon be realized. The bulk SWNT material produced by present methods is an entangled mat of SWNT bundles (known as ropes) made of tubes packed into polycrystalline triangular arrays.

Well before they could be produced in quantity, it was appreciated that the electronic nature of SWNT's is controlled by the precise wrapping of the graphite sheet, due to the latter's critical band structure, poised delicately between metal and semiconductor.[4,5] Later work demonstrated that tube curvature and shape fluctuations have a strong impact on the electronic and transport properties of SWNT's.[6,7] Even small twists strongly backscatter electrons propagating along a tube, while bends in the tube act as much weaker scatterers.

Resistivity measurements of bulk SWNT material and individual ropes agree in large degree with calculations of the electron scattering due to thermally excited twists of intrinsically metallic tubes.[7] At elevated temperature, both bulk and rope resistivities increase linearly with temperature as predicted, but there is a still-mysterious transition to insulatorlike behavior (i.e., $dR/dT<0$) below a crossover temperature that depends on sample preparation. It has been suggested[6] that the source of this crossover could be the onset of backscattering from twist quenched in the samples.

Structural and electronic investigations of SWNT's provide little insight on this issue so far. Extensive TEM,[8] x-ray diffraction,[3] electron nanodiffraction,[9] and Raman-scattering[10] measurements, among other methods, suggest that the samples used in our work, produced by laser ablation at 1200 °C,[11] contain a significant fraction of achiral armchair tubes with diameter near 1.4 nm. Because of their limited spatial resolution, these techniques give little information about the precise atomic configuration of individual tubes. Scanning tunneling microscopy can address this issue,[12,13] but to date no experiments have shed light on the atomic configuration of SWNT's packed into ropes, where tube-tube interactions likely play an important role.

In this paper, we present images of SWNT's within a rope with sufficient spatial resolution to determine the wrapping vector[5] and structural distortions that we attribute to forces exerted by their neighbors in the lattice. Our scanning tunneling microscopy (STM) images could be ascribed to a chiral nanotube, but are more consistently explained as an armchair tube with a quenched twist distortion. We argue that the amount of observed twist can be qualitatively explained within existing theories of SWNT mechanics. Our data is evidence that quenched twists exist in SWNT's in ropes and may contribute to the observed insulatorlike conductivity at low temperature.

In order to get well-defined, atomically flat substrates for high-resolution STM images, we evaporate gold onto mica substrates at 300 °C. After annealing in a gas flame, atomically flat Au(111) terraces several hundred nanometers in size are obtained. As-grown nanotube material was sonicated for 30 min in dichloroethane, then a small drop of the solution was put on the gold surface and blown dry in a nitrogen stream.

Measurements were taken in air with commercial Pt-Ir tips and an STM of the Besocke design (the Beetle STM from Omicron, Inc.). Although the instrument has a rather small scan size of about 2 μm, it allows a reliable coarse lateral movement with steps in the range of 50 to 200 nm, making it possible to find useful sample regions in a few minutes, even with low SWNT density. Lateral dimensions were calibrated to an estimated accuracy better than 15% using atomically resolved images of Au(111), highly oriented pyrolytic graphite (HOPG), and decanethiol monolayers on Au(111). The vertical scale was calibrated at monoatomic steps between terraces of Au(111). Images were obtained with tunneling voltages in the range of 700–900 mV and setpoint currents between 350 and 900 pA. No significant influence of the voltage polarity was noticed.

Figure 1 shows a densely packed rope with a rectangular cross section. It is unclear whether this shape is due to the rope-substrate interaction or if rectangular ropes with such large aspect ratios form during the growth process.[14] At the sidewall of the rope, distinct steps and terraces are seen. A careful examination reveals that the step heights are rather well quantized, implying that the rope consists of tubes with a narrow diameter distribution. This image also lets us accurately determine the direction of the tube axes.

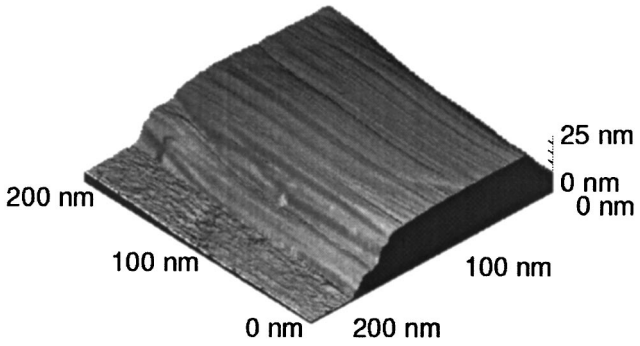

FIG. 1. Image of a rectangular SWNT rope on a Au(111) substrate. Individual tubes are seen on the top of the rope, along with single and multiple tube steps on the near face.

All high-resolution images discussed below were taken with the fast scan direction nearly parallel to the tube axis. This minimizes the effect of lateral tip-sample forces that are found to disrupt the binding between tubes and substrate. Moreover, the amplitude of height changes during each line scan is minimized, resulting in reduced feedback error.

Figure 2(a) shows a high-resolution image of an area on top of the rope. This image combines data from two sequential scans, a procedure made possible by the STM system's low drift. A cylindrical tube is visible, embedded in a flat, disordered surface that may be conducting amorphous carbon. On the surface of the tube we resolve individual hexagons of carbon atoms arranged in the honeycomb lattice of a single sheet of graphite. This honeycomb pattern differs distinctly from the hexagonal lattice typical of STM images of HOPG, where the tip senses only every second atom in a unit cell (the one lying above an atom in the second layer of the *AB* stacked crystal). The distance between the centers of the carbon rings is 0.25 nm, as expected for graphite, confirming the claim that we image each atom on the tube.

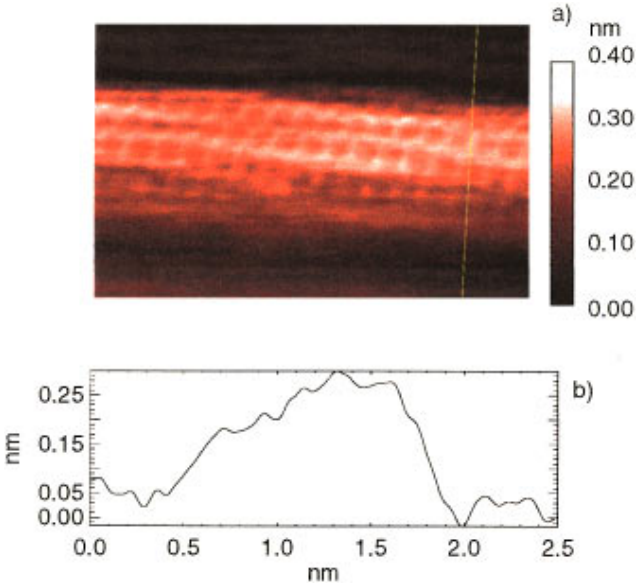

FIG. 2. (a) (Color) High-resolution STM image of an area on top of the rope. Hexagons of carbon atoms are clearly resolved. The hexagon-hexagon distance is 0.25 nm, as expected for a tube rolled from a single graphite sheet. (b) Line scan perpendicular to the tube axis as shown by the white line in (a).

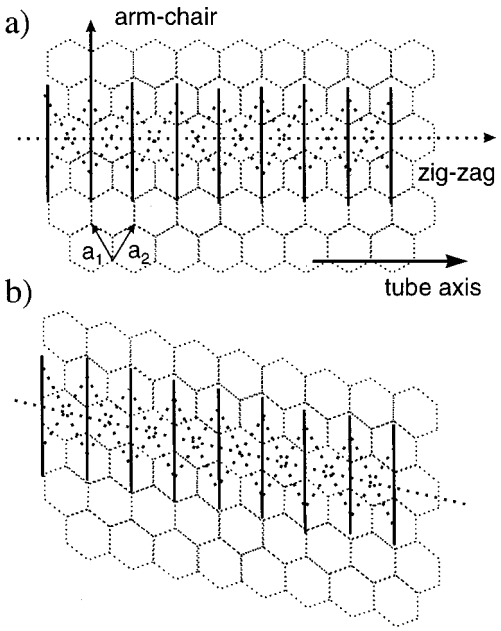

FIG. 3. (a) Sketch of an undistorted armchair nanotube. $\boldsymbol{a_1}$ and $\boldsymbol{a_2}$ are the unit vectors of the graphite lattice. The armchair and zigzag directions are shown by solid and dotted lines, respectively. (b) Sketch of the atomic positions in a twisted armchair tube. The armchair and zigzag directions are indicated as in (a).

Figure 2(b) shows raw topographic data along a line perpendicular to the tube axis. The deviation from a circular cross section likely results from a slightly asymmetric tip shape. The visible tube width is 1.4 nm, and its height above the amorphous background is 0.35 nm. Assuming a circular tube cross section, this gives a measured tube diameter of 1.7 nm. X-ray diffraction data[3] show a rope lattice spacing of 1.7 nm and a peak in the SWNT diameter distribution at 1.4 nm. Since STM probes the electronic rather than nuclear tube diameter, it is not surprising that our measured diameter is close to the rope lattice spacing, since both include a contribution from the electron cloud surrounding the tube.

Following Refs. 4 and 5, we index a SWNT by a pair of integers (n,m) corresponding to the wrapping vector $\boldsymbol{L} = n\boldsymbol{a_1} + m\boldsymbol{a_2}$ that defines the elementary orbit around the tube waist. We also define the armchair and zigzag directions

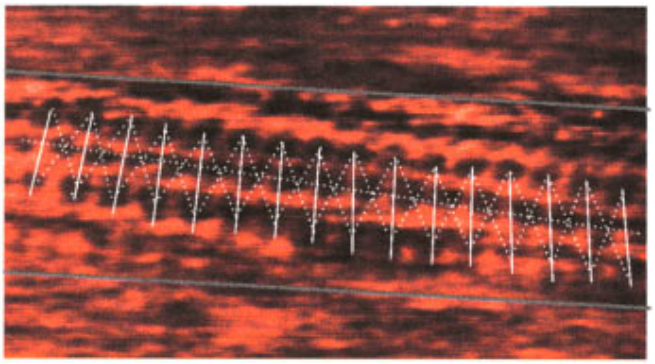

FIG. 4. (Color) Image of the same area as in Fig. 2. The overall tube curvature has been removed to increase the apparent atomic corrugation. The dotted (solid) lines indicate the zigzag (armchair) directions, as in Fig. 3. Two gray lines mark the edge of the tube.

(n,n) and $(n,0)$. Each nanotube index (n,m) has a characteristic diameter and chiral angle between the zigzag direction and the tube axis. For example, the chiral angle of an undistorted armchair tube [see Fig. 3(a)] with wrapping vector (n,n) is zero, since the armchair (solid lines) and zigzag (horizontal dotted arrow) directions are perpendicular and parallel to the tube axis, respectively. Two sets of dotted parallel lines in Fig. 3(a) show the other zigzag directions.

We can take the data from Fig. 2(a) and suppress the tube curvature for enhanced atomic contrast. This yields Fig. 4, where we indicate the tube axis and armchair and zigzag directions as in Fig. 3(a). In Fig. 4 there is a chiral angle of about 4^o between the axis and the zigzag direction, which, combined with the 1.4 nm diameter found above, gives a tentative identification of a (12,9) tube (diameter 1.43 nm, chiral angle 4.7 °). Although this conclusion may be correct, it does not account for all features of the image. Closer inspection of Fig. 4 reveals that the armchair direction is on average perpendicular to the tube axis, as expected for a *nonchiral* armchair tube. In addition, the average angle between the armchair and zigzag directions is greater than 90 °, implying that the tube is *distorted* from its equilibrium conformation.

All these observations can be explained if the images are in fact of an armchair tube with a twist distortion of 4 °. The observed diameter near 1.4 nm would make it a (10,10) tube, although the (11,11) diameter is within experimental error. As sketched in Fig. 3(b), a twist deformation of an armchair nanotube causes the angle between the zigzag and armchair directions to differ from 90 °, while the armchair direction remains perpendicular to the tube axis, just as in Fig. 4. Such distortions are particularly important to the electronic properties of the tube (and rope). A localized twist is a strong source of electron backscattering, and a uniformly twisted SWNT has a gap at the Fermi energy, even if the undistorted tube is metallic.[6] Following Ref. 6, we find that a uniform 4 ° twist of a (10,10) tube creates a gap of 0.6 eV. The splay in the armchair lines of Fig. 4 may indicate a gentle bend of the tube within the rope. As mentioned above, such bends are predicted to have only a minor effect on the rope resistivity.

Although a 4 ° twist is large, it is consistent with what is known about the mechanical properties of SWNT's. Amazingly enough, SWNT mechanics can be modeled rather well as if the tube were a continuous cylinder with a wall thickness of 0.34 nm, the interplane spacing in graphite.[15,16] A tube in a rope will try as much as possible to align its hexagons with those of neighboring tubes as in the *AB* stacking of graphite. In a rope containing tubes of differing helicities, frustration will induce tube twists. Countering this tendency is the energy cost associated with an elastic twist distortion. Little is known about the details of this energy balance and possible energy barriers that define local energy minima. Since ropes produced by laser ablation form within a high-temperature plasma that is rapidly quenched, there could be substantial population of nonequilibrium geometries. Large twists could occur even in ropes made entirely of tubes with the identical wrapping vectors.

We now estimate the magnitude of twist that could be induced by interactions between tubes of differing helicities. Mentally unrolling the SWNT reveals that a twist distortion of a tube is equivalent to a shear of the underlying single plane of graphite [see Fig. 3(b)] whose modulus we take from bulk graphite as $M_b = 0.45$ TPa. Similarly, a rotation of the tube away from its equilibrium alignment with its neighbors in the rope likely has a modulus similar to that of a shear distortion along the graphite c axis, $M_c = 0.004$ TPa. For a (10,10) tube, which is invariant under a rotation of $\pi/5$, the maximum angular deviation from ideal alignment that can occur is $\pi/10$. Since the tube radius is 0.7 nm, the equivalent shear for two graphite planes separated by 0.34 nm is about $e_{max} = 0.67$. The energy stored per unit volume under a shear is the product of the relevant modulus and the square of the shear. This implies that an upper limit on the twist that can occur for the tube is $e_{max}\sqrt{M_c/M_b} = 0.067$. Even larger twists are possible if they are caused by included impurities in the rope. Our observed twist of 4 ° (0.07 rad) is quite close to this estimated upper limit for twists induced by tube-tube interactions alone.

We have achieved atomic STM resolution on 7 samples of SWNT rope material, with reproducible, repeated imaging of between 1 and 8 tubes from each sample, for a total of roughly 30 tubes. In a large fraction of the tubes we see atomic lattices whose bond angles and lengths differ significantly from the expected honeycomb lattice, indicating the presence of twist and shear distortions. It is very unlikely that STM artifacts are responsible for the features we observe. We first consider artifacts due to a finite tip diameter. An ideal zero-radius tip images the projection of the tube on the substrate plane; a tip with nonzero radius stretches the image perpendicular to the axis of the circular tube. Distortions due to a symmetric tip should be symmetric to the center axis of the tube and will not create an apparent twist. An asymmetric tip would lead to an image with distortions depending on the local slope of the tube surface; again this would not be interpreted as a twist.

Tube motion due to forces exerted by the STM tip may also distort the image. Because the tube surface is strongly curved, we expect this force to be nearly perpendicular to the tube axis, and largest when the STM tip is positioned just off of the tubes center. We have observed large tube shifts in our experiments that typically appear as a sudden jump in the image. Slower, more continuous tube motions that lead to distorted images might also occur. To rule out this effect, we took images of the region in Fig. 4 at scan angles as large as 15 ° with respect to the tube axis. They were essentially identical to those presented here, indicating that forces exerted by the STM do not disturb the imaging.

In summary, we have obtained STM images that allow the determination of the atomic structure of an armchair SWNT with a twist distortion from its equilibrium structure in isolation. Additionally, we find that tubes with twist and shear distortions occur generically in as-grown SWNT material. Tube twist should be taken into account when assigning wrapping vectors to SWNT's, and might also occur in individual tubes that are strongly adsorbed on substrates.[13] Quenched twists are expected to strongly affect the intrinsic electronic properties of SWNT's, and they may contribute to the observed insulatorlike resistivity of SWNT ropes at low temperature. Useful future experiments include quantifying the twist frequency in SWNT ropes produced by different techniques (laser ablation versus carbon arc), and determin-

ing whether twist relaxation plays a role in processing techniques (e.g., alkalai doping[7]) known to increase the conductivity of SWNT material.

We thank the Smalley group of Rice University for providing the SWNT material used in these experiments, J. Lefebvre for his assistance with the sample preparation, and C.L. Kane and E.J. Mele for valuable discussions. This work was supported by Penn's Laboratory for Research on the Structure of Matter. W.C. thanks the Deutsche Forschungsgemeinschaft for support. A.T.J. was supported by the David and Lucile Packard Foundation.

---

*Permanent address: Institute for Applied Physics, University of Tuebingen, Tuebingen, Germany. Electronic address: clauss@tuebingen.de

[1] S. Iijima, Nature (London) **354**, 56 (1991).

[2] P.M. Ajayan and T.W. Ebbesen, Rep. Prog. Phys. **60**, 1025 (1997).

[3] A. Thess, R. Lee, P. Nikolaev, H. Dai, P. Petit, J. Robert, C. Xu, Y. H. Lee, S. G. Kim, A. G. Ringler, D. T. Colbert, G. E. Scuseria, D. Tomanek, J. E. Fischer, and R. E. Smalley, Science **273**, 483 (1996).

[4] N. Hamada, S. Sawada, and A. Oshiyama, Phys. Rev. Lett. **68**, 1579 (1992).

[5] R. Saito *et al.*, Appl. Phys. Lett. **60**, 2204 (1992).

[6] C. L. Kane and E. J. Mele, Phys. Rev. Lett. **78**, 1932 (1997).

[7] C. L. Kane, E. J. Mele, R. S. Lee, J. E. Fischer, P. Petit, H. Dai, A. Thess, R. E. Smalley, A. R. M. Verschueren, S. J. Tans, and C. Dekker, Europhys. Lett. **41**, 683 (1998).

[8] P. Nikolaev, A. Thess, A. G. Rinzler, D. T. Colbert, and R. E. Smalley, Chem. Phys. Lett. **266**, 422 (1997).

[9] J. M. Cowley, P. Nikolaev, A. Thess, and R. E. Smalley, Chem. Phys. Lett. **265**, 379 (1997).

[10] A. M. Rao, E. Richter, S. Bandow, B. Chase, P. C. Eklund, K. A. Williams, S. Fang, K. R. Subbaswamy, M. Menon, A. Thess, R. E. Smalley, G. Dresselhaus, and M. S. Dresselhaus, Science **275**, 187 (1997).

[11] T. Guo, P. Nikolaev, A. Thess, D. T. Colbert, and R. E. Smalley, Science **243**, 49 (1995).

[12] K. Sattler, Carbon **33**, 915 (1995); M. Ge and K. Sattler, Appl. Phys. Lett. **65**, 2284 (1994).

[13] J. W. G. Wildöer, L. C. Venema, A. G. Rinzler, R. E. Smalley, and C. Dekker, Nature (London) **391**, 59 (1998); T. W. Odom, J. L. Huang, P. Kim, and C. M. Lieber, *ibid.* **391**, 62 (1998).

[14] J. Lefebvre, R. Antonov, and A. T. Johnson, Appl. Phys. A: Mater. Sci. Process. (to be published).

[15] Jian Ping Lu, Phys. Rev. Lett. **79**, 1297 (1997).

[16] B. I. Yakobson, C. J. Brabec, and J. Bernholc, Phys. Rev. Lett. **76**, 2511 (1996).